Journal of Photochemistry and Photobiology A: Chemistry 222 (2011) 159–165

Contents lists available at ScienceDirect

Journal of Photochemistry and Photobiology A: Chemistry

journal homepage: www.elsevier.com/locate/jphotochem

Antimicrobial activity of Fe–TiO_2 thin film photocatalysts

U. Arellano[a], M. Asomoza[a,*], F. Ramírez[b]

[a] Departamento de Química, Universidad Autónoma Metropolitana-Iztapalapa, Mexico
[b] Departamento de Biotecnología, Universidad Autónoma Metropolitana-Iztapalapa, Av. San Rafael Atlixco No. 186, Iztapalapa, Mexico D.F., Mexico

ARTICLE INFO

Article history:
Received 3 February 2011
Received in revised form 29 April 2011
Accepted 26 May 2011
Available online 2 June 2011

Keywords:
Fe–TiO_2 sol–gel photocatalyst
Escherichia Coli
TiO_2 thin films
Sol–gel
Anatase
Rutile
Visible radiation

ABSTRACT

Fe–TiO_2 sol–gel thin film photocatalysts were prepared by the spin-coating method. Precursory Fe–TiO_2 films, containing 3 and 5 wt.% Fe, were thermally treated at 400 and 800 °C; the dominant crystalline phases of TiO_2 were anatase and rutile, respectively. The thin films were characterized by X-ray diffraction, UV–vis spectroscopy, and scanning electron microscopy. The antimicrobial photocatalytic activity over colonies of *Escherichia coli* bacteria, deposited on the thin films and induced by the incidence of visible radiation was evaluated by the plate counting method. The thin film containing 5 wt.% Fe and treated at 800 °C had a microcrystalline texture and could eliminate *E. coli* bacteria completely after 60 min. In these materials the active phases are both anatase and rutile.

© 2011 Elsevier B.V. All rights reserved.

1. Introduction

Surface chemistry investigation has been significantly increasing as it is shown by the numerous studies that have been recently performed about this topic. Many studies in surface chemistry deal with activated materials and, indeed, the thermal activation of surface processes on diverse substrates is currently a driving force behind a myriad of technological applications.

Electronic excitation is another source of surface activation, which can be induced by absorption of electromagnetic radiation. The electronic activation of surface species has become the first step for developing a new surface chemistry on various materials. Exploration concerning the electronic activation of surface processes is now a very actively and recurring research front line and, in the future, it will grow significantly in interest with respect to sunlight employment for producing electricity and to create and apply new photocatalytic surfaces [1].

Because of its outstanding properties and applications, titanium dioxide (TiO_2) is up to date the most important semiconductor for photochemically decomposing environmental pollutants in order to diminish the harmful effects of these compounds in air or water. TiO_2 is a non-toxic material and is capable to oxidize several compounds under UV irradiation. Many studies about the photodecomposition of pollutants by this metal oxide are currently under way and the preparation of highly effective photocatalysts that are activated by UV radiation has already been pursued [2]. The semiconducting and insulating properties that these solid materials possess are mostly due to the convenient value of their energy band gap (Eg); nevertheless, only a few semiconductors are suitable for photoactivation since Eg for insulators is too large to allow absorption of visible light. Eg is then a very important parameter given that it enables excited electrons to remain in a high energy level for a relatively long period of time thus allowing a fine exploitation of the material properties [3].

Under UV photoexcitation, valence electrons absorb energy thus generating electron hole pairs ($e^- - h^+$) in the valence and conduction bands. Each $e^- - h^+$ pair can diffuse and recombined among themselves in the TiO_2 bulk volume or surface. These $e^- - h^+$ entities have both strong reducing and oxidizing activities and can react with water and oxygen to yield active species, such as hydroxyl radicals ($^\bullet OH$) and superoxide anions (O_2^-). Electron–holes, $^\bullet OH$, and O_2^- are extremely reactive after contacting organic compounds. The oxidation of bacterial cell components, such as lipids and DNA, by these species can produce cell death [4].

The control of dangerous emissions to the environment and the degradation of pollutants are important topics that should be taken into account when trying to reduce the affectations produced by pollution. For the elimination of microorganisms or organic pollutants, several methods such as biological digestion and chemical oxidation are now widely applied. Nevertheless, these methods are not very effective, thus it is important to develop new materials and novel technologies for allowing an improvement of the

* Corresponding author. Tel.: +52 55 58044669x4669; fax: +52 55 58044666.
E-mail address: mjap@xanum.uam.mx (M. Asomoza).

1010-6030/$ – see front matter © 2011 Elsevier B.V. All rights reserved.
doi:10.1016/j.jphotochem.2011.05.016

performance regarding the processes of environmental decontamination [5–7].

Photocatalysis together with the development of effective photocatalytic materials are excellent alternatives for eliminating pollutants in air and water. The degradation mechanism can be activated with UV and visible radiation without generating secondary residual products [8,9].

Thin films are an important option for the treatment of water and air, these materials can eliminate pathogen agents (bacteria, viruses, and other microorganisms) as well as dangerous organic compounds hence leading to their total mineralization [10–14].

The aim of this study is to investigate the antibacterial activity under visible-light irradiation of Fe-doped TiO_2 thin films loaded with 3 and 5 wt.% of Fe; these films, deposited on sodium glass by the spin-coating method, are a fine alternative for the *Escherichia coli* (*E. coli*) water disinfection treatment. The Eg value of these thin films was determined from the UV–vis spectra of these materials. The thin film having 5 wt.% of Fe reached the lowest Eg, as well as a microcrystalline domain texture that was suitable for fine bacterial adherence to the surface. The photocatalytic reaction, induced by visible radiation, and the detection of viable and unviable *E. coli* bacteria were studied. Bacterial concentrations were determined by the standard method of counting the microbe number that was grown on a plate.

2. Experimental

2.1. Synthesis

Fe–TiO_2 thin films were prepared by the spin-coating method, using a burnished Na glass substrate that was treated with concentrated HF in order to improve the adhesion between them. The material to be deposited on the sodium glass substrate was previously synthesized as follows: a volume of 39 mL of ethanol was placed in a glass reactor and subjected to magnetic agitation; afterward, 39 mL of titanium ethoxide, $Ti(OC_2H_5)_4$, and an aqueous solution of $Fe(NO_3)_3{\cdot}9H_2O$ were dropwise added to obtain materials with either 3 or 5 wt.% Fe on TiO_2. The reactant system was adjusted to pH 3 through the addition of diluted HCl, while kept under stirring until all hydrolysis and condensation reactions were accomplished [15]. Subsequently, the resultant gel was filtered, washed with deionized water, and dried at 100 °C. The powder samples obtained this way were labeled as: Fe–TiO_2 3 and Fe–TiO_2 5. When these materials were thermally treated at 400 °C an asterisk was added (i.e. Fe–TiO_2 3* and Fe–TiO_2 5*); similarly, two asterisks were added to the labels of the samples treated at 800 °C (i.e. Fe–TiO_2 3** and Fe–TiO_2 5**). The procedure selected to deposit thin films on glass substrates was the spin-coating method. This was made via a SEVE SC-1000 commercial device. The film formation conditions were chosen as follows: 45 °C, a temperature measured in situ by means of an IR sensor thermometer, and a spinning speed of 700 rpm. On top of a burnished sodium glass substrate, 1 mL of a TiO_2 colloidal suspension was deposited dropwise in order to form a thin film over the glass. After some solvent evaporation, the film was annealed at 400 °C in order to improve its adherence to the glass substrate. The colloidal TiO_2 suspension was prepared as follows: a certain amount of photocatalyst powder that was previously synthesized by the sol–gel procedure was kept under stirring and refluxed at 70 °C, in a 50/50 (v/v) mixture of ethanol and water at pH 10 during 48 h. The suspension thus obtained was used to form the thin film on the glass substrate by repeating twelve times the deposition procedure (one deposition after another) described above.

The resultant thin film samples were labeled, depending on the annealing temperature to which the powder photocatalyst was subjected as: F Fe–TiO_2 3*, F Fe–TiO_2 3**, F Fe–TiO_2 5*, F Fe–TiO_2 5**; the * symbol means a temperature of 400 °C and the ** symbol represents a temperature of 800 °C (in the text it is already stated that the digits 3 and 5 represent the wt.% Fe in the samples).

The average film porosity could be determined by measuring the film apparent density in the following way. The substrate is weighed before the deposition of the film, and then the film and substrate are weighed together. From the values of the film thickness and weight, the apparent density can be calculated. Nevertheless, in the present work, the average-size bacteria, i.e. the rod-shaped *E. coli* is about 0.5 μm in diameter and 2 μm in length; these dimensions easily surpass any actual pore diameter that could be present in the film. Therefore, in this case, bacteria are more likely to remain on the external film surface than to penetrate in its interior and therefore porosity of the film plays no major role.

2.2. Characterization

2.2.1. X-ray diffraction

The X-ray diffraction patterns (XRD) of the Fe–TiO_2 thin film specimens were obtained with a Siemens D500 diffractometer coupled to a Cu anode tube with. The desired Cu-K_α ($\lambda = 1.5406$ Å) radiation was selected by using a diffraction beam monochromator [16].

To study the microcrystalline coating characteristics of the TiO_2 film deposited on glass substrates, the grazing incidence X-ray diffraction (GIXRD) technique was used [17,18]. In this GIXRD technique, the angle of incidence of the X-ray beam with respect to the sample surface is kept fixed at a low value while changing the 2Θ diffraction angle. This procedure allows an enhancement of the diffracted signal coming from the thin film, thus revealing detailed information about sample microstructure; the Bragg reflection width increases due to microstructural features, microcrystal distribution, microcrystal shape, and shrinking of the crystallite sizes.

2.2.2. UV–vis spectroscopy

The UV–vis spectra were obtained via a Cary 100 UV–vis spectrophotometer. From these spectra, the energy band gap (Eg) was calculated.

2.2.3. Scanning electron microscopy (SEM)

Images of the films were obtained with a DSM-940 Carl Zeiss scanning electron microscope, with 30 kW of acceleration voltage and a resolution of 6 nm. The materials were previously coated with gold, using a SCD050 Baltec device. The SEM image magnification was set at 5000×.

2.2.4. Photocatalytic activity

The photocatalytic activity of the Fe–TiO_2 thin films was evaluated in liquid medium inside a stirred photoreactor containing a Luria–Bertani (LB) bacteria culture medium. The photoreactor consisted of a Pyrex glass beaker of 250 mL. The thin film photocatalyst and the liquid culture medium were put inside the beaker and then stirred during the microbial degradation process. The radiation source was a Kr UVP Pen Ray 90-0014-01 lamp that was immersed in the beaker; the radiation emitted by the krypton lamp corresponded to the visible interval of the electromagnetic spectrum. To avoid any kind of interference radiation, coming from other sources, measurements were made in a black walls container. Bacterial photodegradation was carried out at 37 °C, under atmospheric pressure, while dry air was bubbled constantly (1 mL/min) during 1 h.

The photocatalyst film was a square thin layer of 5 cm × 5 cm, with an average thickness of 718 nm that was evaluated by oscillation interferometry [Smith D.L. Thin film deposition Principles & Practice] while applying the Uv–vis spectroscopic procedure

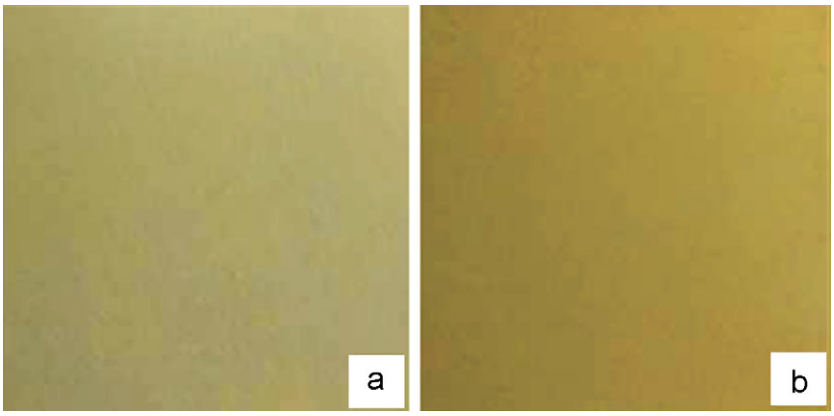

Fig. 1. Thin film images of: (a) F Fe–TiO_2 3* and (b) F Fe–TiO_2 5*.

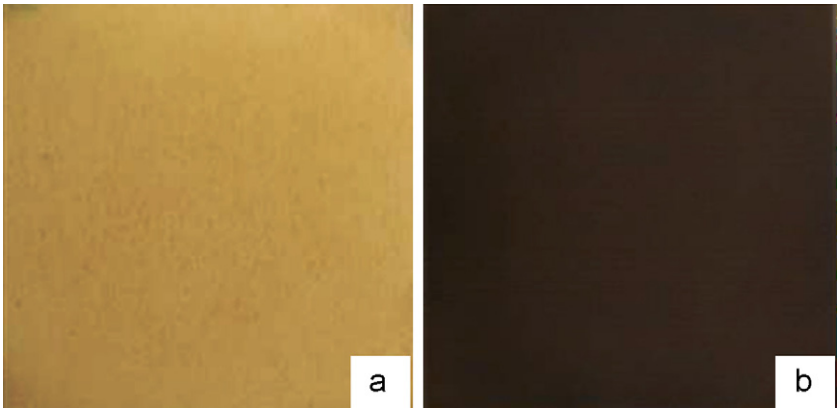

Fig. 2. Thin film images of: (a) F Fe–TiO_2 3 ** and (b) F Fe–TiO_2 5 **.

developed by Swanepoel [19], which is based on the radiation transmitted through a thin absorbing film on a transparent substrate. An average mass difference of 43 mg was determined before and after a thin film was deposited on the glass substrate.

These considerations about the measurement of the film thickness, together with the evaluation of the apparent density, are related to the possibility of assessing the porosity characteristics of the thin film.

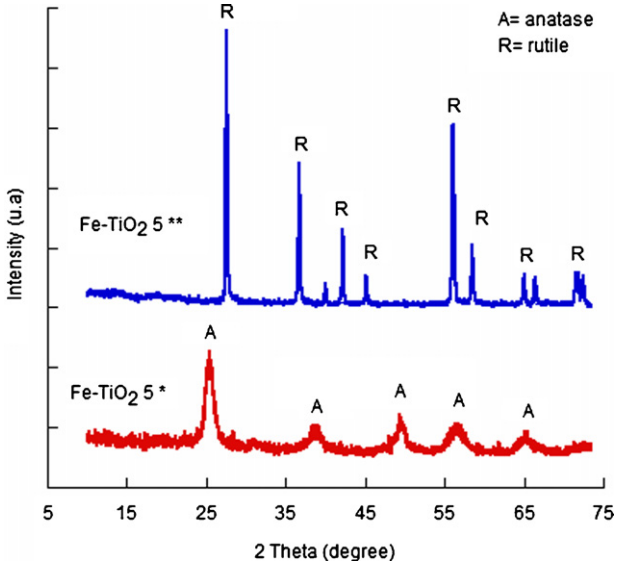

Fig. 3. XRD patterns of precursory powders Fe–TiO_2 5* and Fe–TiO_2 5**.

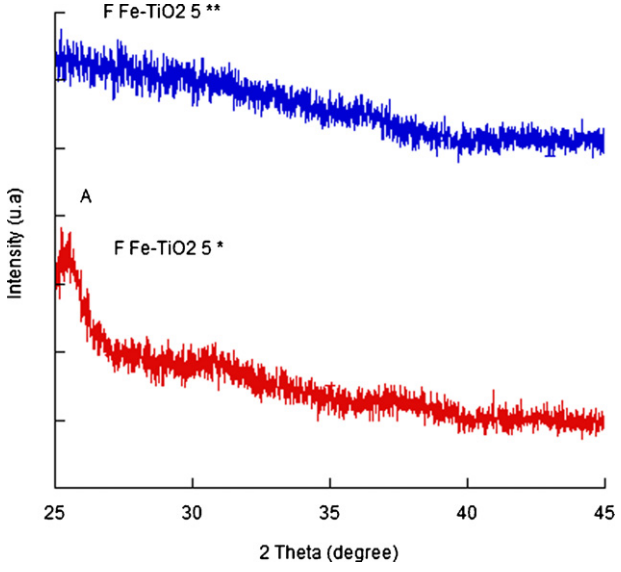

Fig. 4. Thin film GIXRD patterns of F Fe–TiO_2 5* and F Fe–TiO_2 5** thin films.

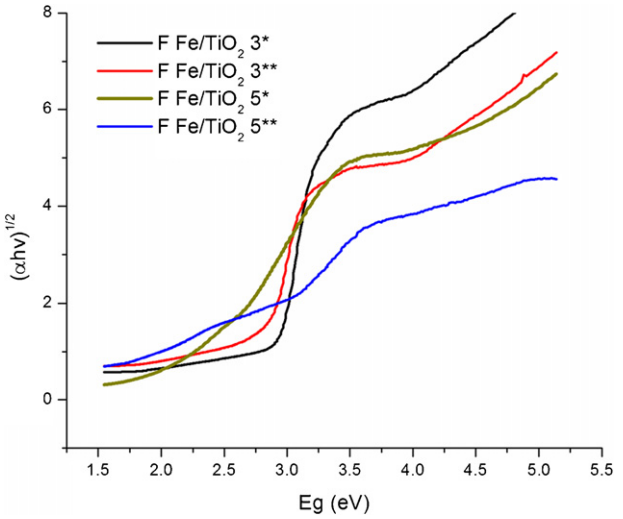

Fig. 5. Uv–vis spectra of F Fe–TiO_2 3*, F Fe–TiO_2 5*, F Fe–TiO_2 3 **, and F Fe–TiO_2 5** samples.

3. Results and discussion

3.1. Synthesis

Fig. 1 shows color photographs of the F Fe/TiO_2 3* and F Fe/TiO_2 5* thin films, obtained from the respective powders. The difference in coloration intensity between the two samples is due to their different Fe contents.

Fig. 2 corresponds to color photographs of F Fe/TiO_2 3** and F Fe/TiO_2 5**, thin films, obtained from their respective powders. The different coloration of the films, if compared to those in Fig. 1, can be attributed to the Fe oxidation state existing at 800 °C (i.e. Fe^{3+}) at which these samples were subjected.

Transition metal oxide preparation procedures [20], cannot avoid the formation of large defect concentrations. In the system Fe–TiO_2, the metal ions preferential oxidation states correspond to Ti^{4+} and Fe^{3+}. However, O vacancy defects can be induced by the Fe content together with the thermal treatment thus reducing these ion oxidation states to Ti^{3+} and Fe^{2+}; indeed, the extent of defects can sometimes be related to the ease of oxidation or reduction processes in transition metals.

3.2. X-ray diffraction

Fig. 3 shows the XRD patterns of the Fe–TiO_2 5* and Fe–TiO_2 5** powders. The dominant crystalline phases present in the calcined materials corresponded to anatase (A) and rutile (R), respectively. The positions of the diffraction peaks match the positions of powder diffraction file (PDF) cards 4-0477 (anatase) and 21-1276 (rutile) (PDF).

Fig. 4 shows the GIXRD patterns of the F Fe–TiO_2 5* sample measured from 25° to 45° 2Θ values; in this case, anatase microcrystalline structure remains after colloidal formation and thin film deposition. For the F Fe–TiO_2 5**sample, the film formation process has led to smaller microcrystals so that the GIXRD signal shows the increased Bragg reflection width ought of to the microcrystalline surface structure. In both diffractograms, the signal from the substrate is completely excluded. The microstructure of the obtained films is not affecting the physical properties of the materials, as well as the Eg values after the film deposition process.

Table 1
Energy band gap.

Sample	Eg (eV)
F Fe–TiO_2 3 *	2.8
F Fe–TiO_2 3 **	2.6
F Fe–TiO_2 5 *	2.2
F Fe–TiO_2 5 **	1.2

3.3. UV–vis spectroscopy

3.3.1. Eg

The XRD spectral region in Fig. 5 corresponding to the Eg of the studied materials was found to fulfill the Kubelka–Munk equation: $(\alpha h\nu)^{1/2} = A\ (h\nu - \mathrm{Eg})$, in which α is the absorption coefficient of the solid, A is a constant that depends on the material, $(h\nu)$ is the photonic energy [21–23].

An energy absorption equivalent to Eg, generates $e^- - h^+$ pairs in the semiconductor materials and these entities are capable of inducing photocatalytic activity [24,25]. In the present work, Eg values are calculated from the absorption spectra through extrapolation of a straight line toward the energy axis. All samples show spectra with similar radiation absorption values and this can be attributed to the electronic transition from an 2p O orbital to a 3d Ti orbital. In these photocatalysts, the Fe^{3+} content likely modifies the Fermi energy level and induces an Eg shift toward the smallest energy values found in the visible region of the electromagnetic spectrum. Table 1 shows the obtained Eg values [25,26].

3.4. Scanning electron microscopy (SEM)

Fig. 6 shows SEM images of F Fe–TiO_2 3* and F Fe–TiO_2 5* thin films. In Fig. 6a thin film particles are seen adhered to the Na sub-

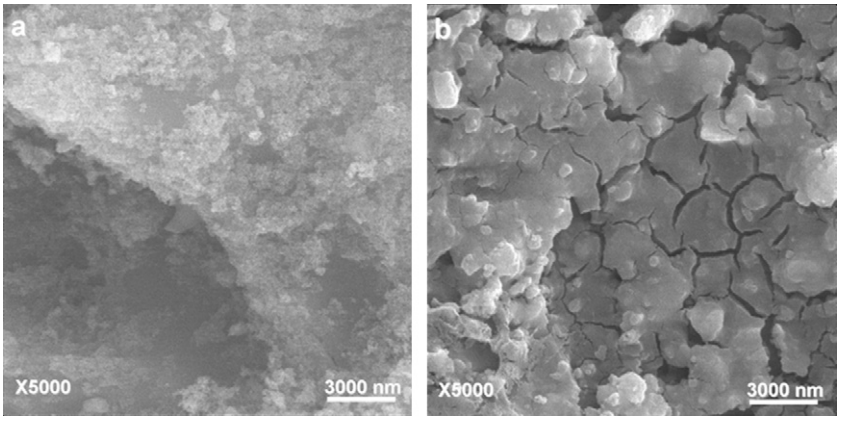

Fig. 6. Thin film SEM images of: (a) F Fe–TiO_2 3* and (b) F Fe–TiO_2 5*specimens.

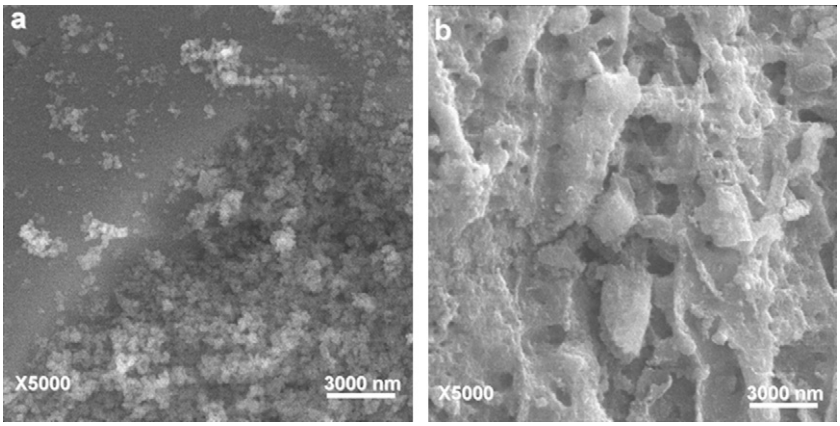

Fig. 7. Thin film SEM images of: (a) F Fe–TiO_2 3 ** and (b) F Fe–TiO_2 5 ** specimens.

strate. In Fig. 6b, it can be noted that the adherence of the Fe–TiO_2 photocatalyst to the glass substrate is poor; in this case, the thin film looks fractured by effect of the of the liquid phase evaporation during film deposition.

SEM micrographs of the F Fe–TiO_2 3** film in Fig. 7a, depicts particles that are adhered to the substrate as an agglomerate; Fig. 7b is a SEM photograph of the F Fe–TiO_2 5** film that presents a texture, which is formed by cavities containing a compact microcrystalline material, this film is the one that presents the best adherence to the Na glass substrate.

3.5. Photocatalytic activity

3.5.1. Growth curve

Fig. 8 shows a typical *E. coli* growth curve. There, an exponential phase growth can be distinguished during 4 h; this can be realized when observing the *E. coli* LB culture medium at 30 min intervals. The bacterial growth rate remains constant and the total population is almost uniform, in regard to the chemical composition of the cells, metabolic activity, and other physiologic characteristics: cells are viable with a constant size. After concluding the *exponential* growth phase, the growth rate rapidly decreases until reaching a standstill; at this point it is said that a *stationary* phase growth has been attained. This phenomenon occurs since the cells have consumed all nutrients and accumulated toxic byproducts by reason of their metabolism.

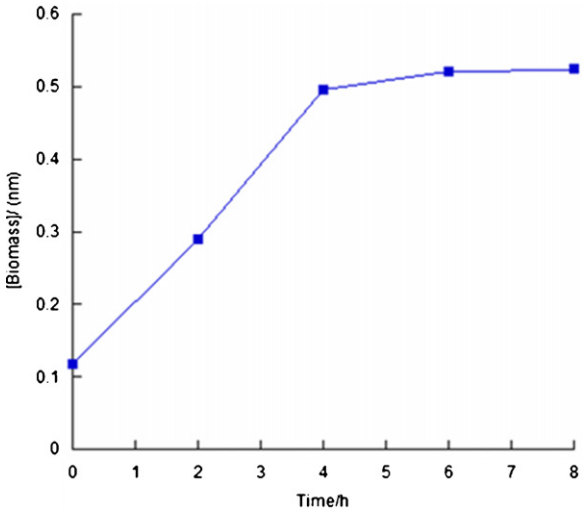

Fig. 8. *E. coli* growth kinetics in LB medium.

A *latency* growth phase is not observed at all since cells arise from an identical medium and are obtained from a fresh culture step that requires no period of adaptation to the new environment.

In the *stationary* growth phase, the number of viable cells remains constant and thus it is possible to evaluate the photocatalytic degradation by starting from the same *E. coli* population. The stationary growth *phase* can be extended up to several hours given that some *E. coli* are divided, others die, and the viable ones continue producing acids and toxic products. Some dead cells are lysed, the cellular membrane is destroyed and cells liberate enzymes (proteases, nucleases, and lipases) that degrade the macromolecules into smaller molecules, those that in turn will be used by the living cells.

The most practical way to distinguish viable and not viable cells after photochemical treatment is by calculating the number of colonies through the plate counting method on a specific solid medium.

Each viable *E. coli* results in the formation of a colony after its incubation in an eosin methylene blue agar (E.M.B) medium, giving a metallic green color characteristic of the colonies. The number of colonies is counted and the result is expressed as colony forming units per milliliter (CFU mL^{-1}) (Fig. 9).

3.5.2. E. coli degradation

Photocatalysis as a disinfection technique implies the influence of the LB medium on *E. coli* degradation; this happens since the medium is a mixture of organic and inorganic substances that improve the bacterial physiological state and increases their

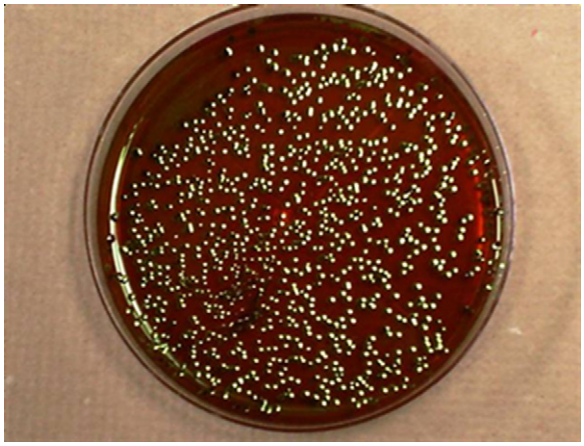

Fig. 9. *E. coli* viable bacteria in E.M.B.

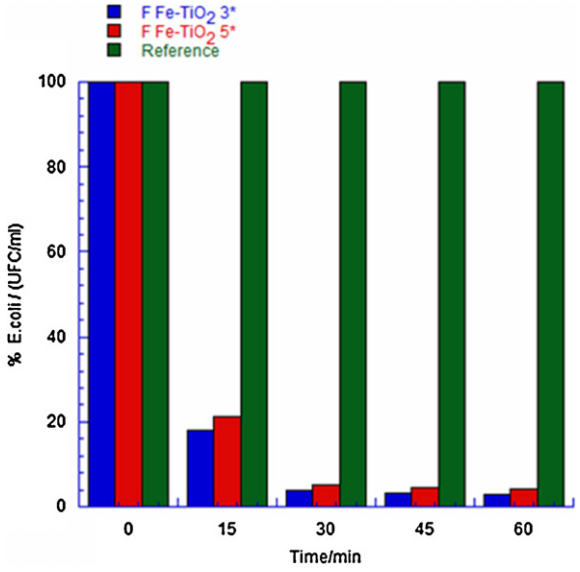

Fig. 10. *E. coli* photodeactivation with F Fe–TiO_2 3* and F Fe–TiO_2 5* thin films irradiated with visible light.

defense mechanisms against the action of light and •OH radicals. The inhibition of the medium implies effects such as: radical scavenging, photocatalyst inhibition, light absorption by the components of the medium, •OH radical competition between the organic compounds of the medium and bacteria, as well as the affinity that exists between these and the photocatalyst. It is then evident the competition existing between the degradation produced by the organic compounds of the LB medium and the microorganisms for photocatalytic disinfection [27,28].

Fig. 10 shows *E. coli* degradation kinetics, under visible light irradiation, for the F Fe–TiO_2 3* and F Fe–TiO_2 5* photocatalysts. The intensity (I) of the applied visible radiation was 0.728 W/m^2, during the first half hour a radiation dose ($I \times t$) of 0.37 Wh/m^2 was applied.

E. coli counting in selective medium, after concluding the photoreaction under visible light, indicated that during the first 30 min only 4 and 5% of the *E. coli* population survives in the presence of the F Fe–TiO_2 3* and F Fe–TiO_2 5* photocatalysts, respectively.

In order to compare photocatalytic activity, a blank test (i.e. that involving no photocatalyst) was employed; after this measurement, it was confirmed that visible radiation has no elimination effect on *E. coli* bacteria [29]. When the radiation dose is duplicated by increasing the exposure time to 60 min, the photocatalysts efficiency increases by 1%, see Fig. 10.

The above described behavior is probably due to the granular surface of the F Fe–TiO_2 3* film since, which is endowed of a low porosity and an Eg of 2.8 eV (Fig. 6a). For the F Fe–TiO_2 5* film, Eg is smaller (Eg = 2.2 eV), see Fig. 6b; however, the texture of this last material is dense and has no porosity since contains multiple fractures due to the evaporation of the precursory solution and its adherence to the substrate is low. Under these conditions, the described samples cannot disable *E. coli* bacteria completely.

Fig. 11 shows the *E. coli* deactivation kinetics in contact with the F Fe–TiO_2 3** and F Fe–TiO_2 5** photocatalysts. When visible radiation is applied during 30 min, only 3 and 1% of *E. coli* survive respectively.

By duplicating the exposure time to 60 min, the photocatalytic activity increased; in the case of the F Fe–TiO_2 3** photocatalyst only 2% of viable *E. coli* remained and with the F Fe–TiO_2 5** sample no bacteria survived. This material and the conditions of this last run allow a total disinfection since microorganisms will no longer be able to reproduce.

The photoactivity of the F Fe–TiO_2 5** thin film shown in Fig. 11 can be attributed to the textural properties and photocatalytic properties of this system, which presents an sinuous texture made of cavities formed by microcrystalline material. It is also worth commenting that defects, oxygen vacancies, Fe content and annealing of Fe–TiO_2 samples produce the overlap between the valence and conduction bands of this system. As the temperature increases, the Eg value decreases toward a lower energy. When the previous bands overlap, metallic conduction starts. If the photocatalysts are irradiated with visible light, $e^- - h^+$ pairs are generated then, as a consequence, •OH radicals are formed. These radicals can attack the membranes of the bacteria adsorbed on the thin film. The smaller activity of the F Fe–TiO_2 3** thin film compared to that of the F Fe–TiO_2 5** material, can be attributed to the difference in the surface texture, where bacteria agglutination per unit area is smaller.

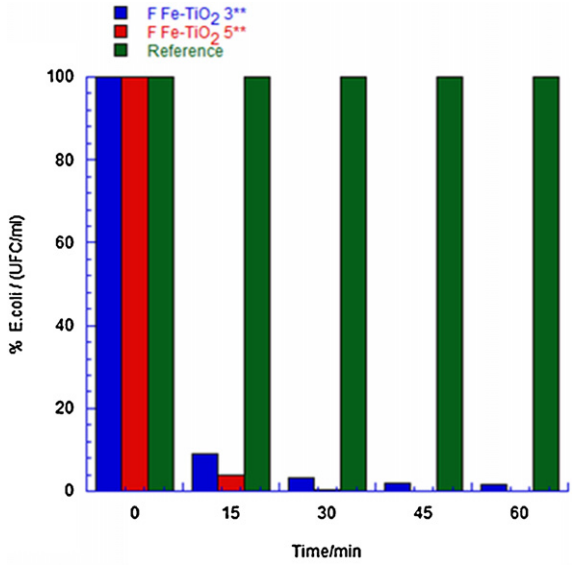

Fig. 11. *E. coli* photodeactivation of with F Fe–TiO_2 3** and F Fe–TiO_2 5** thin films irradiated with visible light.

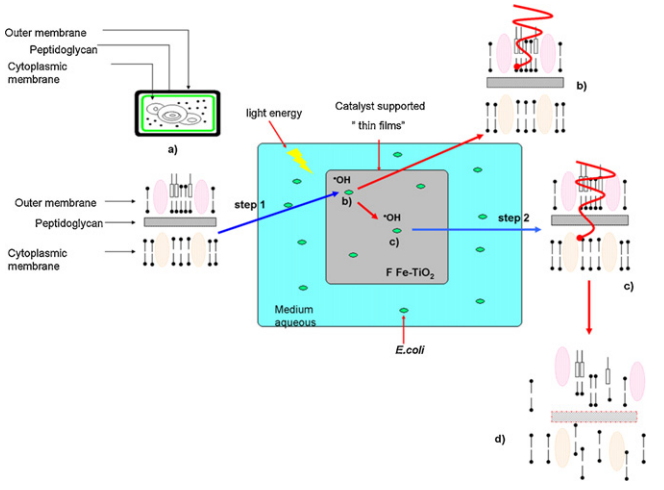

Fig. 12. Scheme of the photocatalytic degradation process of *E. coli* on F Fe–TiO_2 thin films.

3.5.3. Mechanism of E. coli degradation

Fig. 12 schematizes the *E. coli* deactivation process, where: (a) *E. coli* is protected by its external membrane, in this first step, microorganism adhere to the thin film surface; (b) the external membrane is now attacked by the reactive species produced by the photocatalytic effect of the F Fe/TiO_2 thin films; (c) the second step consists of a time period in which the existing species act on the cytoplasmic membrane; (d) in this case, the photocatalytic reaction plays an important role in the introduction of the attacking species through the cell membrane. This would be the reason why *E. coli* die in an effective way over the F Fe/TiO_2 thin films [27,28,30].

4. Conclusions

The photocatalytic activity of TiO_2 semiconductors doped with Fe and activated under visible light conditions is a very promising subject for the elimination of pathogen microorganisms and disinfection of surfaces in order to create self-cleaning areas with application for water disinfection.

The technique devised here for the preparation of thin films is an important one, since the rutile crystalline phase of the doped Fe TiO_2 materials was decreased to microcrystalline size, which involved an energy band gap value that is easily achieved under with visible electromagnetic radiation.

The Fe–TiO_2 thin film photocatalysts developed here are based on the formation of a crystalline rutile phase, which presents an antimicrobial efficiency that results better than those formed from the crystalline anatase phase. This can be attributed, in the first case, to the fact that this material presents a higher contact area for the microorganism adherence and smaller Eg.

Acknowledgements

We wish to thank the Universidad Autónoma Metropolitana-Iztapalapa and the Área de Catálisis of this University for providing financial support and also to the Mexican Science and Technology Research Council (CONACYT) for the support received under Project No. 200394. We also want to thank to technicians Victor Hugo Lara and Patricia Castillo for the XRD and SEM, respectively, for their valuable help.

References

[1] J.T. Yates Jr., Surf. Sci. 603 (2009) 1605.
[2] O. Negishi, K. Takeuchi, J. Sol–Gel Sci. Technol. 22 (2001) 23.
[3] J. Nelson, The Physics of solar cells, Imperial College Press, 2004, p. 43.
[4] M.S. Wong, W.C. Chu, D.S. Sun, H.S. Huang, J.H. Chen, P.J. Tsai, N.T. Lin, M.S. Yu, S.F. Hsu, S.L. Wang, H.H. Chang, Appl. Environ. Microbiol. 72 (2006) 6111.
[5] S. Malato, P. Fernández, M.I. Maldonado, J. Blanco, Catal. Today 147 (2009) 1–59.
[6] R.V. Grieken, J. Marugan, C. Sordo, P. Martínez, C. Pablos, Appl. Catal. B: Environ. 93 (2009) 112–118.
[7] A. Kubacka, M. Ferrer, A. Martínez Arias, M. Fernández García, Appl. Catal. B: Environ. 84 (2008) 87–93.
[8] P.K. Kühn, F.I. Chaberny, K. Massholder, M. Stickler, W.V. Benz, H.G. Sonntag, Chemosphere 53 (2003) 71–77.
[9] P.C. Maness, S. Smolinski, D.M. Blake, Z. Huang, E.J. Wolfrum, W.A. Jacoby, Appl. Environ. Microbiol. 65 (9) (1999) 4094–4098.
[10] J. Wist, J. Sanabria, C. Dierolf, W. Torres, C. Pulgarin, J. Photochem. Photobiol. A: Chem. 147 (2002) 241–246.
[11] M.R. Hoffmann, S.T. Martin, W.Y. Choi, D.W. Bahnemann, Environmental applications of semiconductor photocatalysis, Chem. Rev. 95 (1995) 69–96.
[12] D.M. Blake, P.C. Maness, Z. Huang, E.J. Wolfrum, J. Huang, J. Sep. Purif. Methods 28 (1) (1999) 1–50.
[13] K. Onoda, S. Yoshikawa, Appl. Catal. B: Environ. 80 (2008) 277–285.
[14] W. Xun, G. Wenqi, J. Wuhan Univ. Technol. Mater. Sci. Ed. 23 (2) (2008) 198–202.
[15] M. Asomoza, M.P. Domínguez, S. Solís, V.H. Lara, P. Bosch, T. López, Mater. Lett. 36 (1998) 249–253.
[16] P. Bosch, T. López, M. Asomoza, R. Gómez, Langmuir 11 (1995) 4328–4332.
[17] T. Kyotany, Anal. Sci. 22 (2006) 921.
[18] B.L. Greenberg, D.M. Kalyon, M. Erol, M. Mezger, K. Lee, S. Lusk, Energ. Mater. 21 (2003) 185–199.
[19] R. Swanepoel, J. Phys. E: Sci. Instrum. 16 (1983) 1214–1222.
[20] V.E. Henrich, P.A. Cox, The surface science of metal oxides, Cambridge University Press, 1996.
[21] Y. Wang, A. Suna, W. Mahler, R. Kasowski, J. Chem. Phys. 87 (12) (1987) 7315–7732.
[22] T. López, E. Sánchez, P. Bosch, Y. Meas, R. Gómez, Mater. Chem. Phys. 32 (1992) 141–152.
[23] E. Sánchez, T. López, Mater. Lett. 25 (1995) 271–275.
[24] P. Kubelka, F.A. Munk, Z. Tech. Phys. 12 (1931) 593–601.
[25] R.S. Hunter, R.W. Warold, The Measurement of the Appearance, 2nd ed., John Wiley & Sons, New York, 1987, 142–150.
[26] H.R. Davidson, H. Hemmendinger, J. Opt. Soc. Am. 56 (8) (1966) 1102–1109.
[27] K. Sunada, T. Watanabe, K. Hashimoto, Environ. Sci. Technol. 37 (2003) 4785–4789.
[28] K. Hashimoto, H. Irie, A. Fujishima, Jpn. J. Appl. Phys. 44 (12) (2005) 8269–8285.
[29] K.L. Yeung, W.K. Leung, N. Yao, S. Cao, Catal. Today 143 (2009) 218–224.
[30] K. Sunada, T. Watanabe, K. Hashimoto, J. Photochem. Photobiol. A: Chem. 156 (2003) 227–233.